Editorial Manager(tm) for KSCE Journal of Civil Engineering

Manuscript Draft

Manuscript Number:

Title: Performance Comparison of Spectral Wave Models Based on Different Governing Equations Including Wave Breaking

Article Type: Research Paper

Corresponding Author: Dr. Sang-Ho Oh, Ph.D

Corresponding Author's Institution: Korea Ocean Research & Development Institute

First Author: Sang-Ho Oh, Ph.D

Order of Authors: Sang-Ho Oh, Ph.D; Kyung-Duck Suh, Ph.D; Sang Young Son; Dong Young Lee, Ph.D

Abstract: The performance of three spectral wave models based on different types of governing equations, REF/DIF S, MIKE 21 BW module, and SWAN, was compared by using four laboratory or field experimental data sets. The comparison was focused on accurate prediction of measured wave heights. Characteristics of the three wave models were discussed and their overall predictability of the measured data was evaluated by calculating mean absolute relative errors of wave height. All the numerical models simulated fairly well shoaling and breaking of waves propagating on a plane sloping beach, but the model accuracy was somewhat degenerated in simulating waves propagating over a barred beach. Among the three models, MIKE 21 BW was the most insensitive to the bathymetric change. Combined refraction-diffraction over a shoal without breaking was quite well simulated by the models, especially by REF/DIF S and MIKE 21 BW. When waves break over the shoal, however, all the models failed to reproduce the wave field behind the shoal. The agreement with data in simulating wave diffraction around breakwater was remarkably good for MIKE 21 BW, but poor for other two models. Except the last simulation, the mean absolute relative errors of wave height from the three models ranged between 3 and 27%.

Suggested Reviewers:

Coastal & Harbor Engineering

Performance Comparison of Spectral Wave Models Based on Different Governing Equations Including Wave Breaking

Sang-Ho Oh[a*], Kyung-Duck Suh[b], Sang Young Son[c], Dong Young Lee[d]

[a] *Coastal Engineering & Ocean Energy Research Department, Korea Ocean Research and Development Institute, Ansan 426-744, Korea, ohsangho@kordi.re.kr*
Tel: +82-31-400-7802, Fax: +82-31-408-5823

[b] *Department of Civil and Environmental Engineering & Engineering Research Institute, Seoul National University, Seoul 151-744, Korea, kdsuh@snu.ac.kr*

[c] *Hyundai Institute of Construction and Technology, Hyundai Engineering & Construction Company, Yongin 449-761, Korea, syson@hdec.co.kr*

[d] *Climate Change & Coastal Disaster Research Department, Korea Ocean Research and Development Institute, Ansan 426-744, Korea, dylee@kordi.re.kr*

ABSTRACT

The performance of three spectral wave models based on different types of governing equations, REF/DIF S, MIKE 21 BW module, and SWAN, was compared by using four laboratory or field experimental data sets. The comparison was focused on accurate prediction of measured wave heights. Characteristics of the three wave models were discussed and their overall predictability of the measured data was evaluated by calculating mean absolute relative errors of wave height. All the numerical models simulated fairly well shoaling and breaking of waves propagating on a plane sloping beach, but the model accuracy was somewhat degenerated in simulating waves propagating over a barred beach. Among the three models, MIKE 21 BW was the most insensitive to the bathymetric change. Combined refraction-diffraction over a shoal without breaking was quite well simulated by the models, especially by REF/DIF S and MIKE 21 BW. When waves break over the shoal, however, all the models failed to reproduce the wave field behind the shoal. The agreement with data in simulating wave diffraction around breakwater was remarkably good for MIKE 21 BW, but poor for other two models. Except the last simulation, the mean absolute relative errors of wave height from the three models ranged between 3 and 27%.

Keywords: spectral wave model, model comparison, irregular waves, wave breaking, refraction-diffraction

1. Introduction

Accurate modeling of random wave propagation over an uneven bathymetry is an essential prerequisite for design of coastal structures and prediction of nearshore currents and sediment transport. During the last few decades, a number of spectral wave models have been developed to improve the modeling accuracy and a great progress has been made until recently. Most spectral wave transformation models are classified into three categories depending on the governing equations that are employed: the mild slope equation, Boussinesq equation, and the wave action balance equation. Although the theoretical background and target range of application of these governing equations are much different, many wave models based on these equations have been widely applied to resolving practical problems of wave propagation in the coastal zone.

Several researches have been carried out to compare the performance of different wave models. For numerical models of the mild slope equation using finite difference scheme, a comparative study has been carried out by Maa et al. (2000). In their study, the effects of shoaling, refraction, and diffraction of six regular wave transformation models were analyzed, while energy dissipation due to wave breaking was not considered. Lin and Demirbilek (2005) compared the overall performance of two spectral wave models solving the wave action balance equation with an idealized inlet data. However, to the knowledge of the authors, there is no study comparing simulation results of the spectral wave models based on different governing equations including the effects of wave breaking, which is the main interest of the present study.

Three numerical wave models, REF/DIF S (Kirby and Özkan, 1994), MIKE 21 BW module (DHI Software, 2004), and SWAN (The SWAN team, 2007), were selected for the comparison, which are the most widely used wave models in the coastal engineering community. The performance of these models was examined by comparing their calculation with four well-documented data sets obtained from laboratory experiments or field measurements (Vincent and Briggs, 1989; Mase and Kirby, 1992; Briggs et al., 1995; Birkemeier et al. 1997). Since most of the data sets provide only wave height data, the major focus of the comparison was placed on this physical quantity.

2. Brief Description of the Spectral Wave Models

2.1 REF/DIF S

REF/DIF S is a weakly nonlinear combined refraction and diffraction model developed by Kirby and Özkan (1994). By solving the parabolic form of the mild slope equation developed by Kirby (1986), this model can simulate the effects of shoaling, refraction, diffraction, and energy dissipation, while wave reflection and wave-wave interaction are neglected. In REF/DIF S, individual wave components of a given frequency and direction are simultaneously propagated through the computing domain and the statistical wave parameters are calculated after each forward spatial step. Accurate results are restricted to waves propagating on a mild bottom slope within 45° from the mean wave direction.

2.2 MIKE 21 BW

MIKE 21 BW is composed of two wave modules (1DH and 2DH) based on the enhanced Boussinesq equations (Madsen et al., 1991; Madsen and Sørensen, 1992), which can simulate the propagation of directional waves within the depth to deepwater-wavelength ratio of $h/L_0 \leq 0.5$. MIKE 21 BW can simulate the combined effects of almost all wave phenomena occurring in nearshore regions, including wave grouping, surf-beats, and triad wave interactions (DHI Software, 2004). The wave model generates time series of wave trains by the internal wave generation technique and uses the sponge layers to absorb wave energy at the model boundaries where required. In this study, the 2DH (two horizontal dimensions) module was used.

2.3 SWAN

SWAN is a phase-averaged wave model that computes random, short-crested wind-generated waves in coastal regions and inland waters (The SWAN team, 2007). The model is based on the wave action balance equation with various sources and sinks that accounts for generation, dissipation, and wave–wave interactions of waves in deep and shallow waters (Booij et al., 1999). In SWAN, wave diffraction, which is not explained by the original wave action balance equation, is modeled by a phase-decoupled refraction–diffraction approximation (Holthuijsen et al., 2003). This enables its application to the simulation of wave transformation in coastal areas where wave reflection and diffraction are significant, such as wave field around coastal structures. In this study SWAN

verson 40.51 was used.

In Table 1, the main features of the above three spectral wave models are summarized.

3. Comparison of the Numerical Simulation Results

3.1 Shoaling and breaking over constant slope

3.1.1 Experimental Data

Mase and Kirby (1992) conducted experiments in a wave flume of 47 cm water depth. Unidirectional wave trains of Pierson-Moskowitz spectrum were mechanically generated and propagated over a 1:20 slope beach. Figure 1 shows the schematic view of the experimental setup. Water surface elevations of two different types of waves were measured at 12 locations along the flume at water depths of 47 to 2.5 cm. In the present study, the numerical simulation was made for the Case 1 of Mase and Kirby (1992). In this test condition, the peak frequency of the wave spectrum was 0.6 Hz and plunging-type wave breaking occurred on the sloping beach.

3.1.2 Model Setup

The input spectrum at the offshore boundary was generated by using the wave spectrum measured at the first wave gauge, where the water depth was 47 cm. The offshore boundary was placed at 2 m offshore from the beginning of the slope. The directional spreading of the input spectrum was very narrow to model

unidirectional waves (for example, σ_m = 3 in REF/DIF S model). For other two models, the values of corresponding parameters that control the directional spreading were adjusted to represent almost equal directional spreading among the models. In the following simulations, default values were used for all the physical parameters of each wave model unless their specific values were mentioned.

The computational domain for wave propagation was $0 \le x \le 11.35$ m, $0 \le y \le 0.4$ m, and the grid spacing was 0.05 m in both x and y directions. In MIKE 21 BW model, a sponge layer of 50 grids was placed both in front of the wave generation line and behind the shoreline to absorb the wave energy. The wave spectrum was discretized with 25 frequency bins within the cutoff frequency of 2.5 Hz and 60 directional bins for REF/DIF S and SWAN models. The numbers of frequency and directional bins in MIKE 21 BW were designated by the model. The time step in MIKE 21 BW was 0.01 s, which satisfies the Courant stability condition. The model was run for the duration of 250 peak wave periods and the final result was produced using the last 50 waves.

3.1.3 Results

Figure 2 compares the significant wave heights predicted by the three wave models with the experimental data. On the whole, all the models showed good agreement with the experimental data. In some detail, REF/DIF S and SWAN somewhat overpredicted wave heights in the shoaling region, while MIKE 21 BW predicted slightly smaller wave heights in this region. Within the surf zone, meanwhile, REF/DIF S and SWAN showed better agreement with the measurement than MIKE 21 BW. Note that the wave height of MIKE 21 BW is

non-zero at the shoreline because the model considers the effect of wave setup by the moving shoreline scheme implemented in the model. Also, the wave height of SWAN at the depth smaller than 5 cm could not be calculated due to the depth limitation of the model.

3.2 Wave diffraction around breakwater

3.2.1 Experimental Data

Briggs et al. (1995) conducted laboratory experiments of wave diffraction around a semi-infinite breakwater installed in a wave basin of 35 m wide and 29 m long. As shown in Figure 3, the breakwater was located 8.38 m in front of and parallel to the wave generator. The breakwater was 10 cm thick, and 18.22 m long, extending from centerline of the wave generator to the side wall of the wave basin. Water depth was 46 cm and the breakwater crest was 15 cm high from the still water level. To minimize reflections between the breakwater and the wave generator, wave absorber material was piled on the seaward side of the breakwater. The edge of the wave absorber extended diagonally between the breakwater tip and the end of the wave generator to minimize interference with the desired energy. Waves were measured at three radial transects covering 60° sector of the shadow zone in the lee of the breakwater, at intervals of about 76 cm extending out from the breakwater tip to the point of three times of wavelength. The wave measurement locations are shown as solid dots in Figure 3. Among a total of six different wave conditions, the N2 case (H_s = 0.0775 m, T_s = 1.3 s, γ = 20,

σ_m = 10) were selected for the present numerical simulation.

3.2.2 Model Setup

The computational domain was $0 \le x \le 25$ m and $0 \le y \le 27.4$ m with 0.1 m grid spacing in both coordinates. In MIKE 21 BW model, a sponge layer of 50 grids was placed in front of the wave generation line (x = 0 m), behind the end of the computational domain (x = 25 m), and at both sides (y = 0 m and y = 27.4 m). In addition, another sponge layer was placed in the triangular region on the seaward side of the breakwater shown in Figure 3. In REF/DIF S and SWAN models, the wave absorber on the seaward side of the breakwater could not be reproduced. The input spectrum was discretized with 25 frequency components within the cutoff frequency of 2.5 Hz and 60 directional components. The time step in MIKE 21 BW was 0.02 s satisfying the Courant stability condition. The model was run for 400 peak wave periods and the final wave field was obtained by analyzing the surface elevation during the second half of the run.

3.2.3 Results

Figure 4 shows the measured and calculated values of the diffraction coefficient, the ratio of local wave height to the incident wave height, along the three radial transects. The abscissa of the figure is the radial distance from the breakwater tip normalized by the incident wavelength. As shown in the figure, MIKE 21 BW remarkably well predicted the wave diffraction at the three radial transects. REF/DIF S presented a similar trend to the measurement, but it underestimated the diffraction coefficient for all the transects. This implies that

the model allowed less transfer of wave energy behind the breakwater than the measurement. The performance of SWAN was good at the 90° transect, but showed some disagreement with the measurement for other two transects.

In SWAN, the wave field is smoothed to suppress slight wiggles in geographic space that may arise during computation of wave diffraction. Numerically, the diffraction effect is mainly controlled by adjusting values of the smoothing parameter and the number of smoothing steps. During every smoothing step, all grid points exchange wave energy with their neighbors at a rate assigned by the smoothing parameter. In the present simulation, the number of smoothing steps was assigned to be 30, approximately equal to $1/(3\Delta x^2)$, following the recommendation of the model. For the smoothing parameter, we tested six different values between 0 and 0.25 at an interval of 0.05 and found that 0.2 yielded the best agreement with the measurement. The result of SWAN simulation shown in Figure 4 was obtained by assigning the smoothing parameter of 0.2. The value of greater than 0.25 was not tried because it may result in too excessive smoothing of the wave field.

3.3 Combined refraction and diffraction over a shoal

3.3.1 Experimental Data

Vincent and Briggs (1989) made comprehensive measurements of wave deformation over an elliptical shoal installed in a wave tank of 35 m wide and 29 m long. As shown in Figure 5, waves were generated by the spectral wave generator and propagated over the shoal. The center of the shoal, whose radius

was 3.05 m in x direction and 3.96 m in y direction, was located at x= 6.10 m and y= 13.7 m. The water depth was 45.72 cm at the bottom of the tank and 15.24 cm at the center of the shoal. Wave elevation data were collected at 9 locations along the transect at x = 12.2 m behind the shoal (See Figure 5). Among a total of 17 experimental conditions, two cases (N4 and B5) shown in Table 2 were selected for the present numerical simulation.

3.3.2 Model Setup

The computational domain for wave propagation was $0 \le x \le 25$ m and $0 \le y \le 27.4$ m with 0.1 m grid spacing in both coordinates. In MIKE 21 BW model, a sponge layer of 30 grids was placed in front of the wave generation line (x = 0 m), behind the end of the computational domain (x = 25 m), and at both sides (y = 0 m and y = 27.4 m) to absorb the wave energy. The input spectrum was discretized with 25 frequency components within the cutoff frequency of 2.5 Hz and 60 directional components in REF/DIF S and SWAN models. The time step in MIKE 21 BW was 0.02 s satisfying the Courant stability condition. The model was run for 400 peak wave periods and the final wave field was obtained by analyzing the surface elevation during the second half of the run.

3.3.3 Results

Figure 6 shows a comparison of the calculated and measured wave heights along the transect at x = 12.2 m for Case N4. The ordinate in the figure is the local wave height at the transect normalized by the incident wave height. The wave heights calculated by REF/DIF S and MIKE 21 BW agreed fairly well with the

measured heights. In contrast, the result of SWAN showed some difference with the experimental data. In Figure 6, the SWAN result without wave diffraction (Diff off) was also provided to show the effect of wave diffraction in the model. It is clearly seen that wave height increased for all the grid points at the transect when wave diffraction was taken into account in the model. The SWAN result with wave diffraction shown in Figure 6 was obtained by the smoothing parameter value of 0.2, same as in the wave simulation shown in section 3.2. In the present computation, the value of the smoothing parameter was also changed from 0 to 0.25 at an interval of 0.05 as in section 3.2, and the value of 0.2 again produced the best agreement with the experimental data.

Figure 7 shows a similar comparison made for Case B5. In this experimental setup, the incident wave height was much greater than Case N4, so that wave breaking occurred over the shoal. As shown in Figure 7, the measured wave height was distributed as a concave pattern along the transect, higher waves at both sides than the center of the transect. However, this trend was poorly simulated by all the wave models, which predicted almost the same wave heights along the transect. Among the three wave models, the wave heights of REF/DIF S were slightly greater than other two models. In SWAN, the effect of wave diffraction was not so prominent as in the simulation of Case N4.

3.4 Propagation of obliquely incident waves over a barred beach

3.4.1 Experimental Data

Comprehensive data of nearshore currents, waves, wind, tide, and bathymetry

was collected in the barred beach at Duck, North Carolina during the DELILAH field measurement from October 1 to 19, 1990. The bottom topography of the beach is characterized as the planar mild slope with a bar at approximately 50 m seaward from the shoreline. During the field measurement, the bottom bathymetry was surveyed every day over the so-called minigrid area that covers about 550 m in the alongshore direction and 400 m in the cross-shore direction from the shoreline. Meanwhile, waves were measured at the offshore station of 8 m water depth, approximately 800 m seaward from the shoreline, and at nine nearshore locations along the cross-shore line within the range of 250 m from the shoreline. Full details of the field experiment are explained in the report of Birkemeier et al. (1997).

3.4.2 Model Setup

Among the extensive field data available, we selected two conditions for the present simulation as listed in Table 3. The selected test conditions are designated as Case D1 and D2, respectively. The water depth and wave parameters shown in Table 3 are the values measured at the offshore station. In the numerical simulation, the computational domain was constructed to the extent of the offshore wave station, further offshore of the daily surveyed minigrid area. The bottom bathymetry outside the minigrid area was created based on the assumption of a constant bottom slope to the depth of the offshore station. This is justified because the bathymetric change was insignificant outside the minigrid area as reported by Birkemeier et al. (1997). As shown in Table 3, the incident wave angle at the offshore boundary, θ_0, is not perpendicular to the shoreline. Hence, the

computational domain was further extended in the alongshore direction by prolonging the south cross-shore boundary (y = 724 m) to the extent at y = 174 m. Figure 8 illustrates bottom contours of thus created computational domain for Case D1. The coordinates in the figure follow the FRF (Field Research Facility) system. The nine dotted symbols in the figure indicate the locations of nearshore wave measurement.

The computational domain covers $50 \le x \le 914$ m and $174 \le y \le 1274$ m with the grid spacing of 4 m in the longshore direction and 2 m in the crossshore direction. For MIKE 21 BW setup, a sponge layer of 50 grids was placed beforehand the offshore wave generation line (x = 914 m). The input spectrum was discretized with 40 frequency components within the cutoff frequency of 0.5 Hz and 60 directional components in REF/DIF S and SWAN models. The time step in MIKE 21 BW was 0.2 s satisfying the Courant stability condition. The model was run for 100 peak wave periods and the final wave field was obtained by analyzing the surface elevation during the second half of the simulation time.

3.4.3 Results

In Figure 9, the calculated significant wave heights are compared with the measurement for Case D1. Also shown in the figure is the beach profile along the cross-shore transect at y = 984 m, in the range of covering nine nearshore wave measurement locations. Outside the surf zone, the computed wave heights by the three models agreed well with the measurement overall. The wave breaking point, which is located at the seaward slope of the bar, was also predicted relatively well by the three models. SWAN showed the best agreement with the experimental

data, while other two models predicted more shoreward breaking point than the measurement. Meanwhile, apparent differences were found between the calculated results and the measurement inside the surf zone. The energy dissipation rate over the bar was much lower in the numerical models than the measurement. Hence, the predicted wave heights at the bar trough ($x \approx 160$ m) were about 30~40% higher than the measured wave height. The underprediction of surf zone wave height in Case D1 was also reported by Chen et al. (2003) who used the same field data for simulating nearshore waves and longshore current with a different type of Boussinesq model. Meanwhile, the step-like variation of wave height due to the barred bathymetry was not clearly captured in MIKE 21 BW model. Besides, the wave height at the shoreline was non-zero because the effect of wave setup was taken into account in the model.

Comparison of the measured and computed wave heights for Case D2 is shown in Figure 10. In this test condition, the incoming wave height at the offshore boundary is approximately half of Case D1. In addition, the bar trough is less noticeable than the previous test case. As shown in Figure 10, wave shoaling was somewhat overestimated by REF/DIF S and SWAN models. The incipient wave breaking was anticipated to occur at further shoreward location than the measurement. Among the three models, SWAN predicted the most seaward location whereas MIKE 21 BW was opposite to this, which is the same tendency as in Case D1. Inside the surf zone, the measured wave height decreased monotonously without the step-like variation of wave height along the cross-shore line. In contrast, the simulation results of REF/DIF S and SWAN showed the step-like change of wave height inside the surf zone. In MIKE 21 BW, the predicted

wave height decreased without the step-like pattern, but the value was much higher than the measured height.

4. Discussion

4.1 Qualitative comparison of the model characteristics

As shown in Figures 2, 9 and 10, wave shoaling was well simulated in general by all the wave models tested in this study. However, the shoaling wave heights shown in Figure 10 were slightly higher than the observation, especially for REF/DIF S and SWAN. In this test condition, it seems that the simulated wave heights outside the surf zone were also somewhat higher than the observation, which might result in the disagreement of wave height due to wave shoaling. Judging from the simulation results shown in this study, MIKE 21 BW predicts the smallest increase of wave height due to shoaling. Other two models give similar results for wave shoaling.

The location of depth-limited wave breaking was also predicted reasonably well by the three models. Compared to REF/DIF S, SWAN and MIKE 21 BW respectively predicted slightly seaward and shoreward point of incipient breaking. The three models performed relatively well in predicting the decrease of wave height due to wave breaking on the constant sloping bottom as shown in Figure 2. However, the wave energy dissipation rate over the barred beach was much smaller than the field observational results as shown in Figures 9 and 10. Among the three models, surf zone wave height decreased most rapidly in REF/DIF S. In

contrast, MIKE 21 BW predicted the slowest decrease of wave height inside the surf zone. Considering that this model predicted the slowest increase of wave height in the shoaling region, MIKE 21 BW seems to be the least sensitive model to the bathymetric change among the wave models tested in this study.

Wave diffraction was remarkably well simulated by MIKE 21 BW model, which is the most outstanding advantage of the model against the other two models. As shown in Figure 4, the model results almost completely agreed with the experimental data. The diffraction coefficient of REF/DIF S showed almost the same transitional pattern as the measurement for all the transects. However, the model underestimated the magnitude of wave diffraction, especially at the radial transect that made smaller angle with respect to the breakwater. Based on this result, it seems that less wave energy is diffracted into the shadow zone behind the breakwater than the measurement. This may be due to the parabolic approximation used in REF/DIF S, which makes the solution inaccurate as the wave direction deviates from the principal direction. SWAN was similar to REF/DIF S in that its performance becomes worse as the angle between the radial transect and the breakwater becomes small. Judging from the result shown in Figure 4, the ability of SWAN in predicting wave diffraction around the breakwater is comparable to REF/DIF S. Considering that wave diffraction in SWAN is somewhat incompletely implemented by the approximation suggested by Holthuijsen et al.(2003), this result is quite satisfactory.

As shown in Figure 6, the combined refraction and diffraction over the shoal under non-breaking condition was fairly well simulated by both REF/DIF S and MIKE 21 BW models. In contrast, the simulation result of SWAN without wave

diffraction showed apparent disagreement with the measured data in the central region of the transect. This discrepancy occurs mainly because the location of wave focusing would be nearer than the measurement when wave diffraction was not taken into account. When wave diffraction was activated, the wave height increased over the whole transect, which resulted in disagreement of wave heights at both sides as well as the center of the transect. On the whole, SWAN produced more smoothed distribution of wave height behind the shoal than the measurement.

Meanwhile, when wave breaking occurs over the shoal, the measured wave height behind the shoal was distributed as the concave pattern shown in Figure 7. This was not satisfactorily simulated by any of the three models because they do not consider the strong breaking-generated current that defocuses the wave field behind the shoal. Recent researches (Yoon et al., 2004; Choi et al., 2007) have shown that the accuracy in simulating waves breaking over the shoal can be improved by including the effect of breaking-induced currents in REF/DIF S or SWAN models.

4.2 Quantitative evaluation of the model performance

In order to quantitatively compare overall performance of the three spectral wave models, the mean of absolute relative errors of wave height was calculated for all the numerical simulations. The quantity is defined as the percent change of the predicted wave height to the measured wave height as in Lin and Demirbilek (2005).

$$\varepsilon = \frac{1}{N}\sum^{N}\frac{\left|H_s^p - H_s^m\right|}{H_s^m} \quad (1)$$

where ε is the mean of absolute relative errors, N is the number of experimental data, and H_s^p and H_s^m is the predicted and measured wave heights, respectively. The calculated values of ε by the three wave models for all the wave simulations in this study are shown in Table 4.

In comparison with the experiment of Mase and Kirby (1992), the mean of absolute relative errors by the three models ranged from 3.2 to 6.7%. Hence, it can be stated that all the models predict fairly well wave shoaling and breaking over a constant slope.

The simulation of wave diffraction around a breakwater showed significantly different results depending on the wave model. The performance of MIKE 21 BW was good as the values of ε varied only 3.6 to 12.3% for all the transects. In contrast, other two models showed poor agreement of wave height with measurement, particularly for the transect of smaller angle with the breakwater. The errors of REF/DIF S varied from 11.7% to 53.3% while those of SWAN from 6.7% to 38.2%. Note that the errors in SWAN were smaller than REF/DIF S for all the transects.

Combined refraction and diffraction over the shoal without wave breaking was quite well simulated by the wave models. As shown in Table 4, the mean of absolute relative error was only 3.2% for REF/DIF S and 3.6% for MIKE 21 BW. The corresponding value for SWAN was 7.3%, slightly higher than the other two

models. Meanwhile, when the diffraction effect was not considered in SWAN, the error was reduced to 4.8% as indicated in the parenthesis. This was caused by the overall increase of wave height behind the shoal by activating wave diffraction as shown in Figure 6, which resulted in greater absolute relative errors. On the other hand, the errors by the three models slightly increased to the range between 9.2 and 12.3% when wave breaking occurred over the shoal. The greater errors in this test condition are ascribed to the inability of simulating strong breaking-induced current that prevent wave diffraction behind the shoal. Meanwhile, the error in SWAN was reduced by only 0.2% when wave diffraction was deactivated in the model.

The errors in simulating wave propagation over a barred beach by the three models varied in the range of 17.8 to 23.7% for D1 case, whereas 20.1 to 26.7% for D2 case. For the two test cases, the values of ε were not so different among the three models as in the simulation over a constant slope. However, the errors were much greater because the predicted wave heights in the range of the barred bathymetry deviated much from the measurement as seen in Figures 9 and 10.

5. Conclusion

On the whole, the three spectral wave models tested in this study showed good performance in predicting the height of waves propagating over a varying bathymetry although they are based on intrinsically different types of governing equations. The mean absolute relative errors of wave height from the three models ranged between 3 and 27% for all the test conditions except for the case of wave

diffraction around breakwater, for which the most obvious difference was found among the numerical models. MIKE 21 BW was overwhelmingly good in predicting wave heights at the entire radial transects in the shadow zone behind the breakwater. In contrast, the simulation results of REF/DIF S and SWAN were reasonably good at the transect perpendicular to the breakwater, but were deteriorated at other transects whose angle from the breakwater was smaller.

The variation of wave height behind a submerged shoal due to combined refraction-diffraction over the shoal was fairly well simulated by both REF/DIF S and MIKE 21 BW models unless waves break on the shoal. Meanwhile, SWAN predicted less focused distribution of wave height along the transect behind the shoal. Judging from the simulation results of the two different test conditions including wave diffraction, it can be stated that wave diffraction might be successfully simulated by REF/DIF S as long as the bottom varies smoothly so as not to invoke strong wave reflection. In addition, SWAN seems to produce the most smoothed distribution of wave height along the direction perpendicular to wave propagation. When waves break on the shoal, on the other hand, the three wave models were not able to simulate the concave distribution of wave height behind the shoal because none of the models considers the effect of breaking-generated current that defocuses the wave field behind the shoal.

All the numerical models showed relatively good performance in predicting wave shoaling and subsequent breaking on a plane sloping beach. However, the model accuracy decreased in the simulation of obliquely incident waves over a barred beach since the energy dissipation rate inside the surf zone was underpredicted by the numerical models. It might be necessary to further

investigate this feature by using another well-documented field data. Meanwhile, among the wave models tested in this study, MIKE 21 BW showed the most gradual variation of wave height in the direction of wave propagation, which implies the least sensitiveness of the model to the bathymetric change.

Acknowledgements

This research was supported by the Brain Korea 21 project and Korea Ocean Research and Development Institute.

References

Birkemeier, W.A., Donohue, C., Long, C.E., Hathaway, K.K., and BARON, C.F. (1997). *The 1990 DELILAH Nearshore Experiment: Summary Report*. *Technical Report CHL-97-24*, U.S. Army Corps of Engineers, Waterways Experiment Station, Vicksburg, Ms.

Booij, N., Ris, R.C., Holthuijsen, L.H. (1999). "A third-generation wave model for coastal regions. Part I. model description and validation." *J. Geophys. Res.*, Vol. 104 No. C4, pp. 7649– 7666.

Briggs, M.J., Thomson, E.F., and Vincent, C.L. (1995). "Wave diffraction around breakwater." *J. Wtrwy., Port, Coast., and Ocean Engrg.*, *ASCE*, Vol. 121, No. 1, pp. 23-35.

Chen, Q., Kirby, J.T., Dalrymple, R.A., Shi, F., and Thornton, E.B. (2003). "Boussinesq modeling of longshore currents." *J. Geophys. Res.*, Vol. 108, No. C11, 3362, doi:10.1029/2002JC001308.

Choi, J., Lim, C.-H., Jeon, Y.-J., and Yoon, S. B. (2007). "Numerical simulation of irregular wave transformation due to wave-induced current." *J. Hydro-environ. Res.*., Vol. 1, pp. 133-142, doi:10.1016/j.jher.2007.08.001

DHI Software. (2004). *MIKE 21 Boussinesq Wave Modules, User Guide*, DHI Water & Environment, Hørsholm, Denmark.

Holthuijsen, L.H., Herman, A., and Booij, N. (2003). "Phase-decoupled refraction –diffraction for spectral wave models." *Coast. Engrg*., Vol. 49, pp. 291–305.

Kirby, J.T. (1986). "Higher-order approximations in the parabolic equation method for water waves." *J. Geophys. Res.*, Vol. 91, No. C1, pp. 933-952.

Kirby, J.T. and Özkan, H.T. (1994). *Documentation and user's manual, Combined Refraction/Diffraction Model for Spectral Wave Conditions, REF/DIF S, Version 1.1. CACR Report. No. 94-04*, University of Delaware, Department of Civil Engineering, Center for Applied Coastal Research, Newark, Delaware.

Lin, L. and Demirbilek, Z. (2005). "Evaluation of two numerical wave models with inlet physical model." *J. Wtrwy., Port, Coast., and Ocean Engrg.*, *ASCE*, Vol. 131, No. 4, pp. 149-161.

Maa, J.P.-Y., Hsu, T.-W., Tsai, C.-H., and Juang, W.J. (2000). "Comparison of wave refraction and diffraction models." *J. Coast. Res.*, Vol. 16, No. 4, pp. 1073-1082.

Madsen, P.A. and Sørensen, O.R. (1992). "A new form of the Boussinesq equations with improved linear dispersion characteristics. Part 2. A slowly-varying bathymetry." *Coast. Engrg.*, Vol. 18, pp. 183-204.

Madsen, P.A., Murray, R., and Sørensen, O.R. (1991). "A new form of the Boussinesq equations with improved linear dispersion characteristics." *Coast. Engrg.*, Vol. 15, pp. 371-388.

Mase, H. and Kirby, J.T. (1992). "Hybrid frequency-domain KdV equation for random wave transformation." *Proc. 23th Int. Conf. Coast. Engrg. ASCE*, Venice, Italy, pp.474-487.

The SWAN team. (2007). *SWAN User Manual, SWAN Cycle III Version 40.51AB.* Faculty of Civil Engineering and Geosciences, Delft University of Technology, GA Delft, The Netherlands.

Vincent, C.L. and Briggs, M.J. (1989). "Refraction-diffraction of irregular waves over a mound." *J. Wtrwy., Port, Coast., and Ocean Engrg.*, *ASCE*, Vol. 115, No. 2, pp. 269-284.

Yoon, S.B., Cho, Y.-S., and Lee, C. (2004). "Effects of breaking-induced currents on refraction-diffraction of irregular waves over submerged shoal." *Ocean Engrg.*, Vol. 31, pp. 633-652.

Table

Table 1. Summary of the three spectral wave model capabilities.

	REF/DIF S	MIKE 21 BW	SWAN
Governing equation	Parabolic mild slope equation	Boussinesq type equation	Wave action balance equation
Solution method	Phase resolving	Phase resolving	Phase averaging
Refraction	Yes	Yes	Yes
Shoaling	Yes	Yes	Yes
Diffraction	Yes	Yes	Yes (Approximation)
Wave-current interaction	Yes	Yes	Yes
Wave-wave interaction	No	Yes (Nonlinear)	Yes (Triad + Quadruplet)
Whitecapping	No	No	Yes
Wave breaking	Yes	Yes	Yes
Reflection	No	Yes	Yes (Specular)
Transmission	No	Yes	Yes
Dissipation by bottom friction	Yes	Yes	Yes
Generation by wind input	No	No	Yes

Table 2. Input wave parameters of the selected test cases (Vincent and Briggs, 1989).

Case	H_s (m)	T_s (s)	γ	σ_m
N4	0.0254	1.3	20	10
B5	0.1900	1.3	2	30

Table 3. Test conditions of the selected cases of DELILAH experiment.

Case ID	Time & Date	Tide (m)	Depth (m)	H_s (m)	T_s (s)	θ_0 (°)	σ_m	γ
D1	04:00, Oct. 10	-0.29	7.37	1.13	10.7	-34	16	4
D2	04:00, Oct. 06	-0.41	7.80	0.53	12.0	-22	13	6

Table 4. Mean of absolute relative errors (%) of wave height by the three wave models.

Test condition	REF/DIF S	MIKE 21 BW	SWAN
	Shoaling/Breaking over a plane slope		
	6.7	5.2	3.2
	Diffraction around breakwater		
30° transect	53.3	12.3	38.2
60° transect	30.0	3.6	23.0
90° transect	11.7	6.2	6.7
	Refraction-Diffraction over a shoal		
N4 case	3.2	3.6	7.3 (4.8)
B5 case	9.2	12.3	11.8 (11.6)
	Inclined propagation over a barred beach		
D1 case	20.4	23.7	17.8
D2 case	20.1	26.7	23.7

Captions of Figures

1. Sketch of the experimental setup (Mase and Kirby, 1992).
2. Significant wave heights measured from the experiment (Mase and Kirby, 1992) and computed by the three models.
3. Sketch of the experimental setup (Briggs et al., 1995).
4. Diffraction coefficient along the three transects from the experimental data (Briggs et al., 1995) and from the computational results of the three models.
5. Sketch of the experimental setup (Vincent and Briggs, 1989).
6. Normalized wave heights along the transect measured from the experiment (Vincent and Briggs, 1989) and computed by the three models (Case N4).
7. Normalized wave heights along the transect measured from the experiment (Vincent and Briggs, 1989) and computed by the three models (Case B5).
8. Bottom contours of the barred beach for the numerical computation (4:00 AM, on 10 October 1990).
9. Significant wave heights of the DELILAH field measurement and computational results by the three models (Case D1).
10. Significant wave heights of the DELILAH field measurement and computational results by the three models (Case D2).

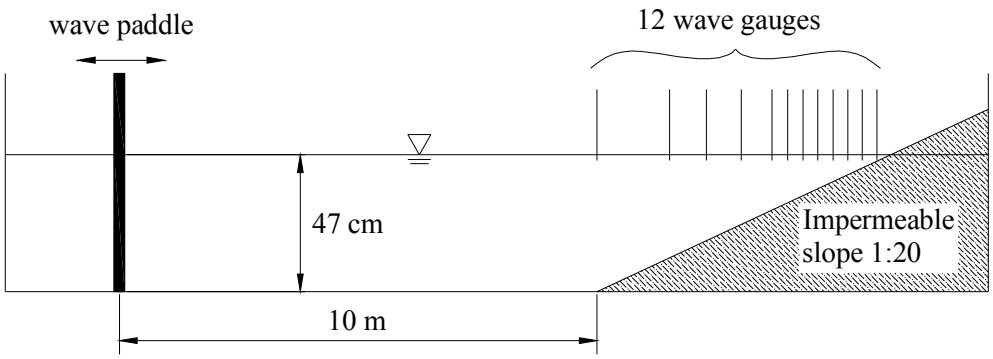

Figure 1. Sketch of the experimental setup (Mase and Kirby, 1992).

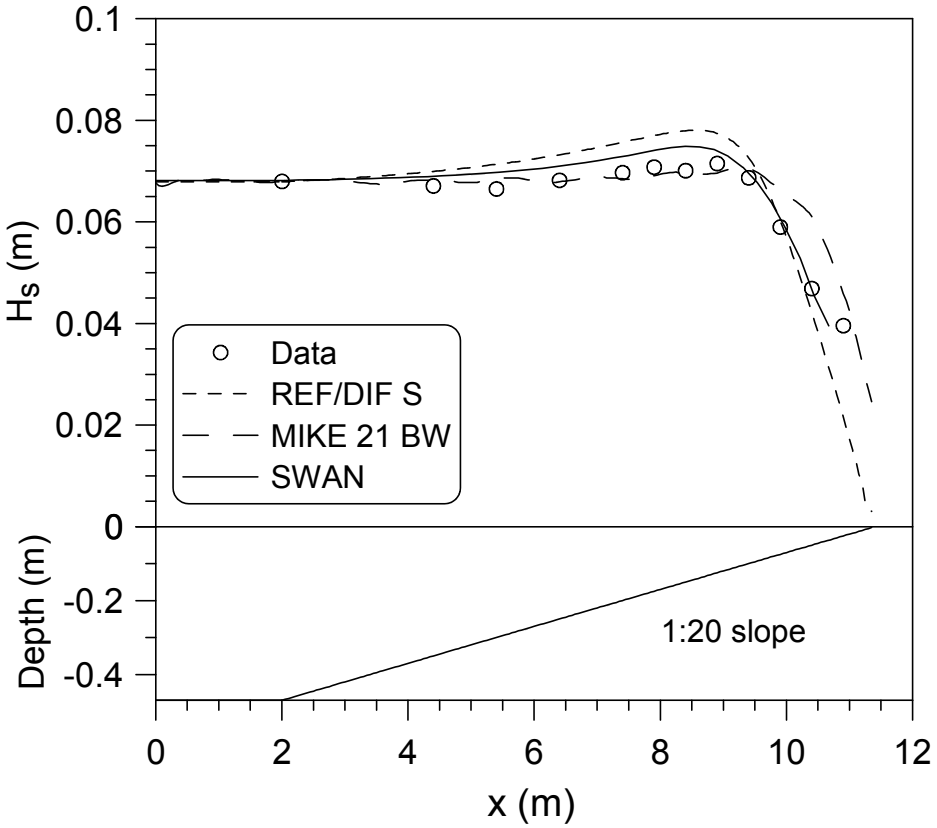

Figure 2. Significant wave heights from the experimental data (Mase and Kirby, 1992) and computed by the three spectral wave models.

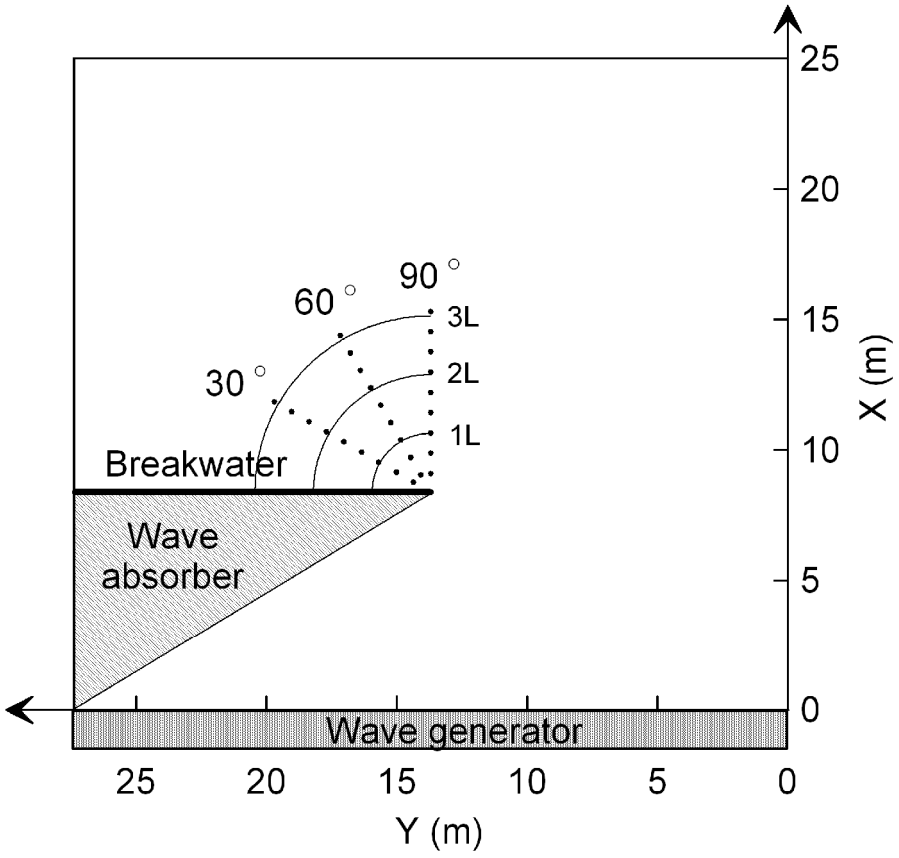

Figure 3. Sketch of the experimental setup (Briggs et al., 1995).

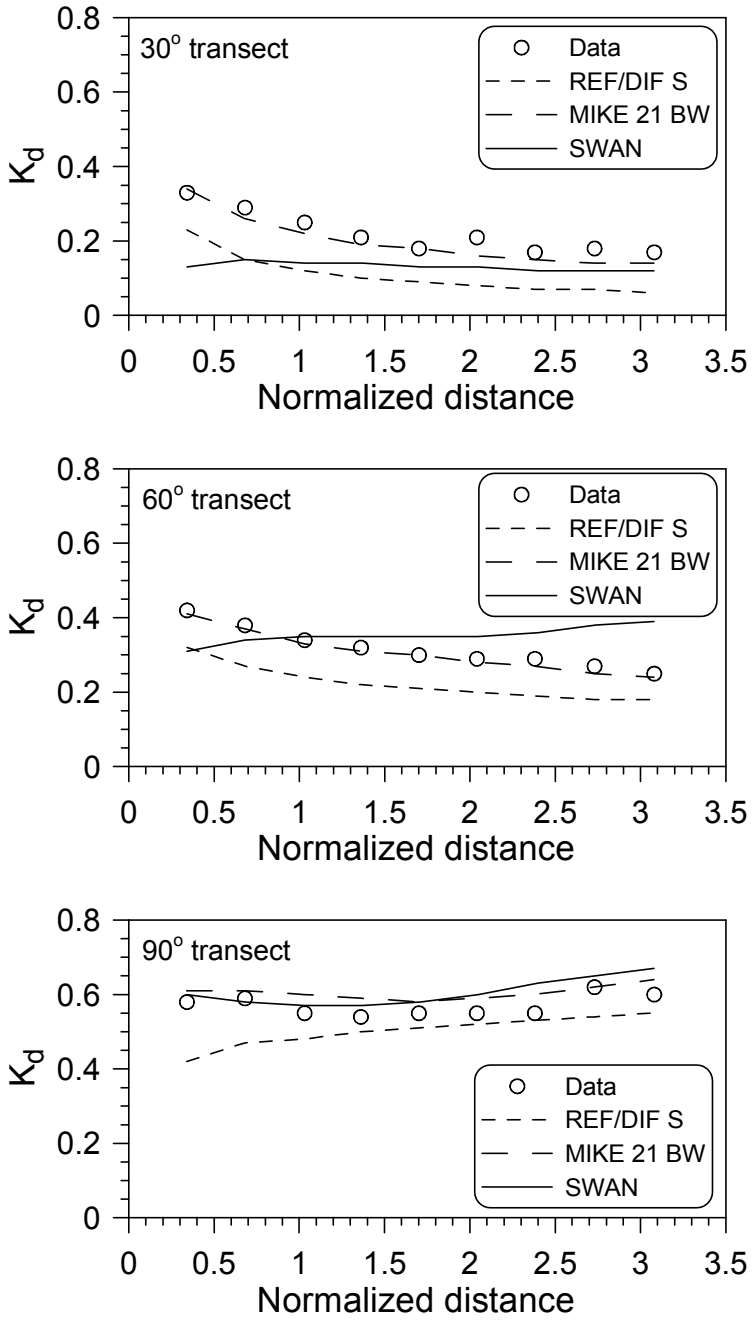

Figure 4. Diffraction coefficient along the three transects from the experimental data (Briggs et al., 1995) and from the computational results of the three models.

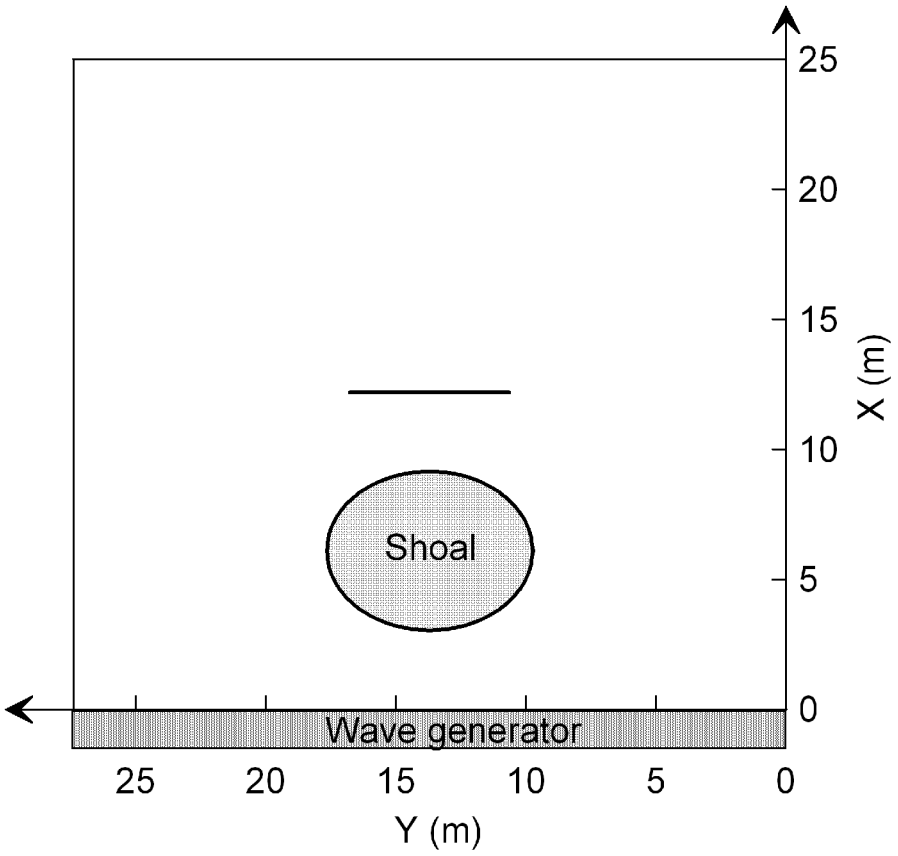

Figure 5. Sketch of the experimental setup (Vincent and Briggs, 1989).

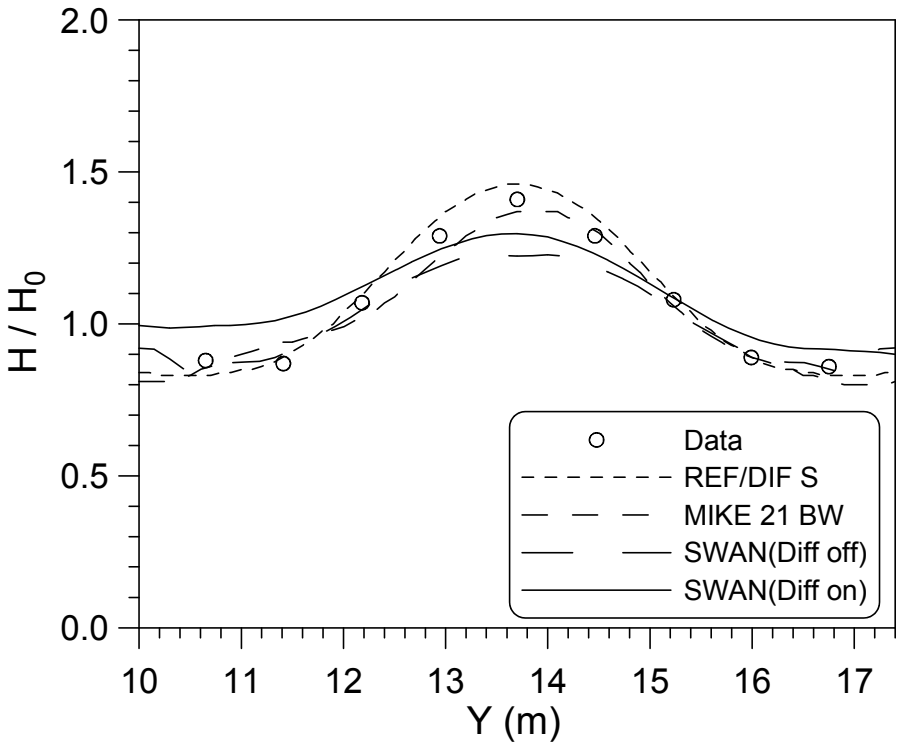

Figure 6. Values of normalized wave height along the transect measured from the experiment (Vincent and Briggs, 1989) and computed by the three models (Case N4).

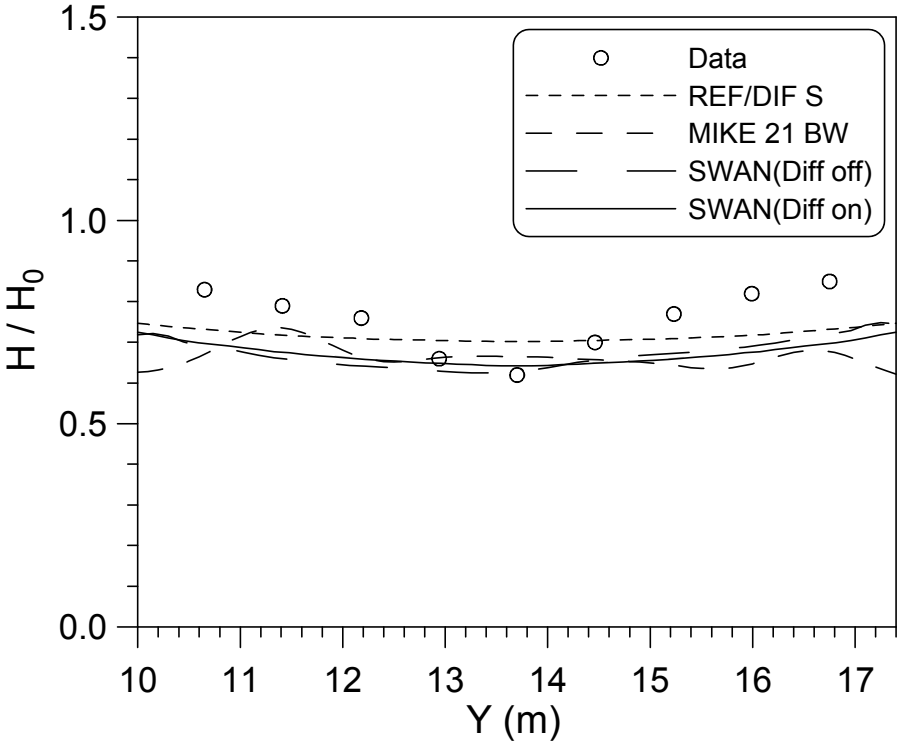

Figure 7. Values of normalized wave height along the transect measured from the experiment (Vincent and Briggs, 1989) and computed by the three models (Case B5).

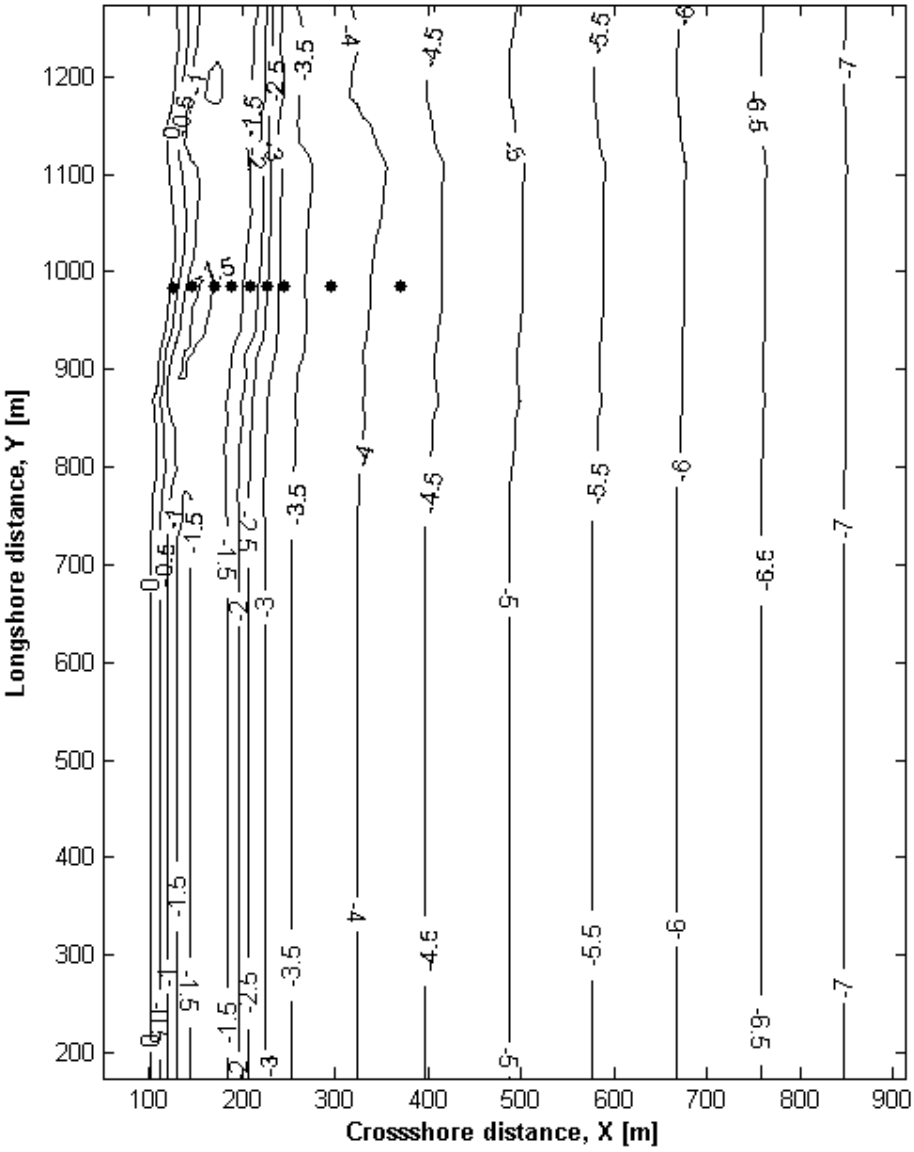

Figure 8. Bottom contours of the barred beach for the numerical computation (4:00 AM, on 10 October 1990).

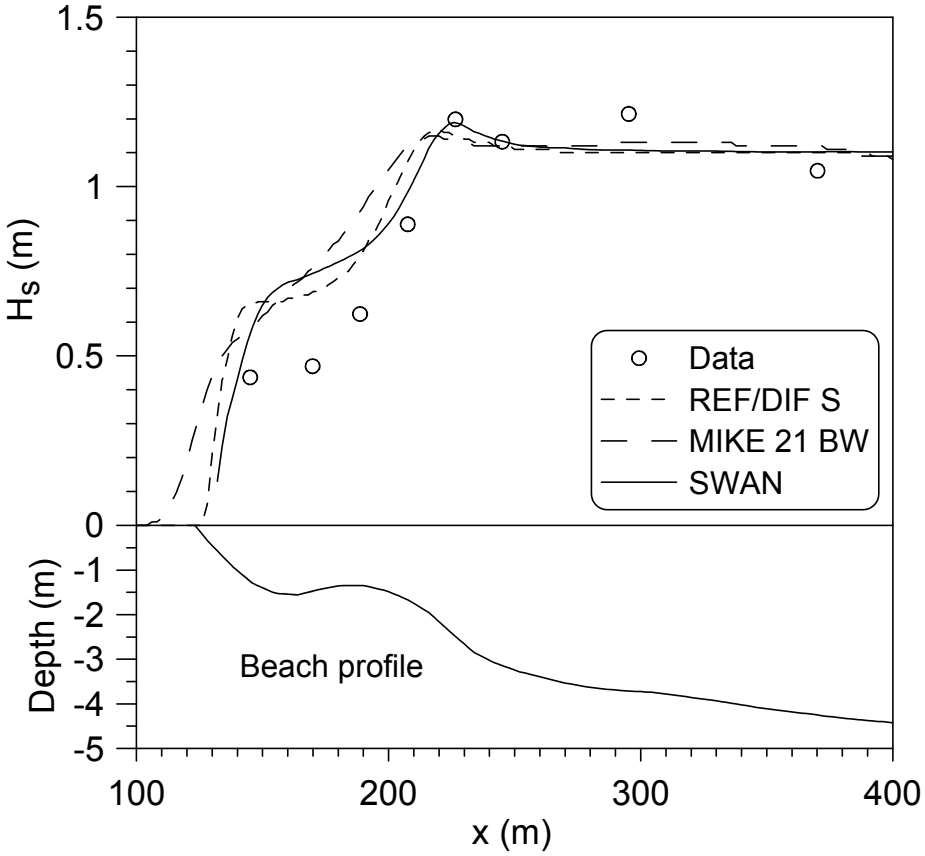

Figure 9. Significant wave heights of the field measurement (Birkemeier et al., 1997) and computational results by the three models (Case D1).

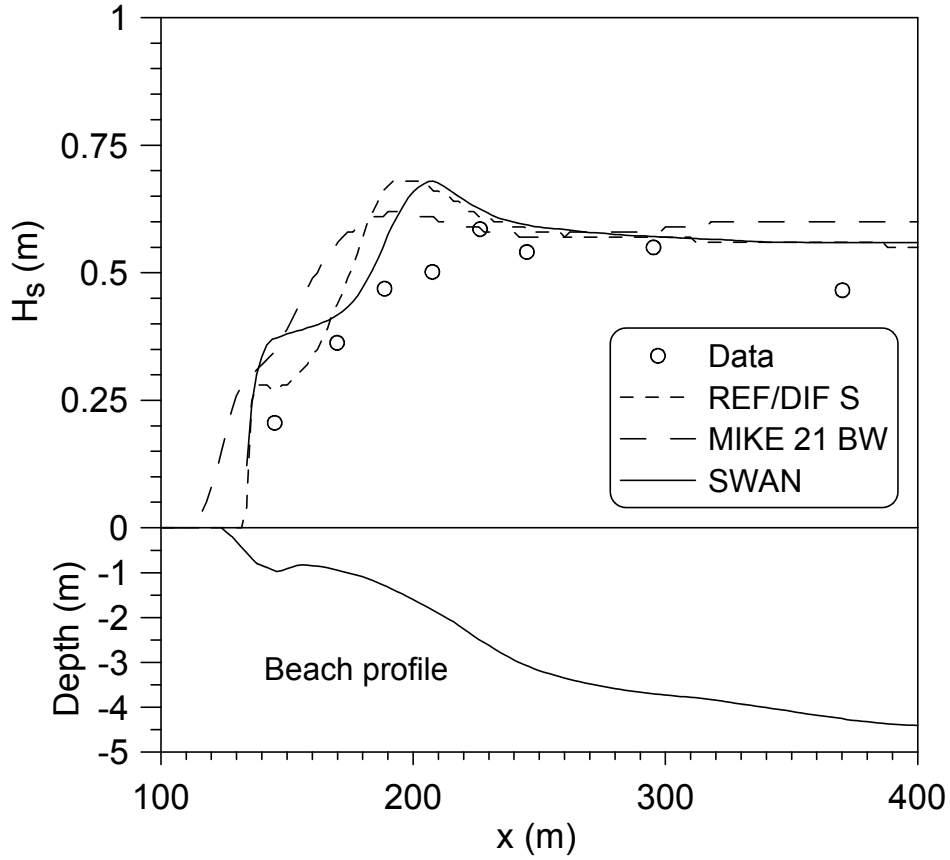

Figure 10. Significant wave heights of the field measurement (Birkemeier et al., 1997) and computational results by the three models (Case D2).